

Super-telephoto Drone Tracking Using HFR-video-based Vibration Source Localization

Nagahiro Fujiwara, Mingjun Jiang,
Takeshi Takaki, and Idaku Ishii
*Department of System Cybernetics
Hiroshima University
1-4-1 Kagamiyama, Higashi-Hiroshima,
Hiroshima 739-8527, Japan
nagahiro-fujiwara@hiroshima-u.ac.jp,
{m-jiang, takaki, iishii}@robotics.hiroshima-u.ac.jp*

Kohei Shimasaki
*Digital Monozukuri (Manufacturing)
Education Research Center
Hiroshima University
3-10-32 Kagamiyama, Higashi-Hiroshima,
Hiroshima 739-0046, Japan
simasaki@robotics.hiroshima-u.ac.jp*

Abstract— In this paper, we propose a super-telephoto drone surveillance system that can search and track a flying drone at a 1 km distance or more within an area spanning hundreds of square meters. By constructing a mirror-drive high-speed pan-tilt control system with a super-telephoto camera lens, remote drone surveillance becomes possible owing to the acquisition of high spatial resolution images of target objects. We adopted a vibration-based drone localization algorithm that can simultaneously detect fast-rotating drone-propellers in an high-frame-rate video using a pixel-level short-time Fourier transform to achieve robust surveillance under various challenging conditions for super-telephoto video-shooting such as low luminance and heat haze. The effectiveness of the super-telephoto drone tracking system is demonstrated by conducting a drone searching and tracking experiment at a 1 km distance using an 800-mm focal length lens with a mirror-drive video-shooting system.

Index Terms— high-speed vision, target tracking, vibration localization, drone surveillance, telephotography

I. INTRODUCTION

Drone technologies have improved all over the world in recent years so that the market for drone technologies is expected to grow sharply. Drones are now used in a variety of aerial applications such as delivery services, disaster investigations, infrastructure maintenance, and farm work assistance due to the improvement in its long-distance flying technology, including automatic remote control and long-lasting batteries. With an increase in the drone market, however, abuse of drones that can fly long distances is occurring; for instance, terrorist attacks on military facilities and delivery of illegal merchandise have emerged as a social problem.

From this kind of circumstance, the anti-drone market is expected to grow from 499 million USD in 2018 to 2276 million USD by 2024 [1]. Most of the anti-drone systems consist of localization and interference technologies. Several approaches to drone interference, including shooting nets at the drone's position and radio-wave jamming have been proposed. However, these technologies require that an exact location of the drone be obtained by other methods. Thus,

localization is a crucial task for any anti-drone system. It is difficult, however, for auto-detection systems to search for small-size drones at long distances in many environments. Hence, many drone localization methods based on a variety of features of flying drones have been proposed.

Vision-based drone-tracking systems based on high-speed propeller rotation [2], [3] have been proposed as a robust drone localization method using high-frame-rate (HFR) video analysis. This research focused on pixel-level time-series variations in which only specific frequency vibration pixels using pixel-level digital filters for particular frequency domains can be detected in an HFR video, whose frame rate is faster than the rotation frequencies of propellers to be detected. By extracting pixels in the range of an assumed propeller rotation frequency band, only the propeller part can be detected in a specific vibration region. In this method, whether a part of a drone's propellers or not, an image can be evaluated at every pixel. Drones can be localized accurately in several challenging conditions such as in small and defocused images, even though humans and other appearance-based methods cannot recognize such unclear objects.

Here, to observe high-frequency waveforms such as a propeller's rotation, high-speed vision systems [4], [5], [6] with HFR video sequences are required. That is, video sequences must be captured at least twice the frame rate and target frequency, according to the Nyquist theorem. For example, the video should be captured at 400 fps or more to measure vibrating objects at 200 Hz. As such, an audio-level frequency visualization system using high-speed vision, real-time vibration spectrum imaging technology [7], and a short-time Fourier transform based on time-series brightness changes over a specific period have been reported. The effectiveness of such a method has been verified through applications such as vibration inspection of industrial products and high-frequency flapping wings feature-based honeybee activity sensing [8].

At the same time, a high-speed vision system can track

high-speed moving objects, due to its high temporal resolution that can enable various algorithms including face detection [9] and convolutional neural network-based (CNN-based) object detection [10] that is performed as a real-time fast-tracking system. Moreover, a mirror-drive tracking system with high-speed vision [11] that can realize 1 ms feedback gaze control shows the usefulness of a high-speed tracking system through a ping-pong ball tracking experiment. Notably, in the case of a telephoto video-shooting system, control rates decrease when a camera platform device is used because of its weight. In contrast, by controlling the angles of small mirrors on the order of ms, high-speed gaze control can be achieved, regardless of the camera's size, weight, and magnification.

In this paper, we propose a remote drone searching and tracking system that combines a propeller vibration extraction algorithm using a short-time Fourier transform [7] and a mirror-drive high-speed tracking system with fast feedback control. Although limited-range images can be captured by a camera at a 1 km distance, our proposed system can search and track drones over a broader range when mirror-drive active vision is installed. Moreover, we demonstrate a real-time flying drone searching and tracking experiment at a 1 km distance and discuss the effectiveness and problems of the proposed algorithm.

II. COMPARISON WITH A CONVENTIONAL APPROACH TO DRONE LOCALIZATION

Every drone surveillance method has both strong and weak points. Radar-based methods [13] can detect flying objects at long distances, but it is difficult for radar systems to separate drones from other objects such as flying birds and airplanes. The radio-frequency-based method can detect some specific frequency bands that flying drones transmit. However, it may not detect new types of drones because it is necessary to know their frequency band beforehand. Audio-based methods [14] utilizing the features of high-frequency propeller sound can detect drones in invisible places, but an accurate position cannot be localized because of the low directivity of acoustic information, and localization accuracy considerably decreases at long distance and a high noise location.

Many vision-based methods have been proposed, and most of them are based on spatial features of frames such as Haar-like features [15] and gradient histograms [16]. Moreover, deep neural network methods, including CNN-based identification [17], have been developed with the improvement of computational power and multi-thread processing technologies including FPGA and GPU computing and availability of a large amount of openly accessible data. Although CNN-based detection accuracy in various challenging conditions such as small images and some noise in the image is higher than other conventional spatial feature-based identification methods, there is a limit to detecting an object in low res-

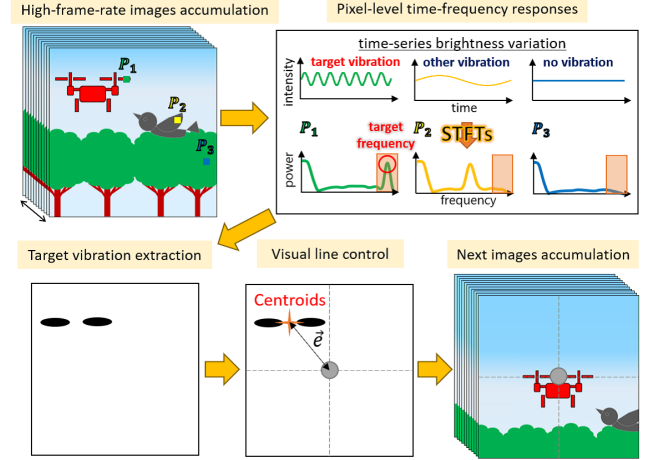


Fig. 1. Mirror-drive drone tracking system with pixel-level vibration extraction.

olution and unclear images because the objects that humans cannot recognize in frames cannot be detected.

Considering that almost all methods have difficulty in localizing remote drones without false detection, propeller vibration-based drone surveillance using high-speed vision is better, especially at long distances, as we mentioned in Section I.

III. SUPER-TELEPHOTO DRONE SEARCHING AND TRACKING SYSTEMS

A. Concept

Figure 1 describes the concept of a vibration-based remote drone surveillance method using a super-telephoto mirror-drive video-shooting system. From the increased demand for wide-area drone surveillance on the order of several kilometers, we constructed a telephoto drone searching and tracking system that can expand the range of view for drone localization. Several camera platform control systems that can move the camera have been demonstrated as a method of expanding the field-of-view, although the control rate decreases when a telephoto lens is used because it is heavyweight. A mirror-drive vision system is needed to control the viewpoint at high-speed regardless of the type of camera and lens. On the other hand, a captured video is affected by heat haze in super-telephoto video-shooting, which causes accuracy deterioration in a spatial feature-based method. That's why we utilized a vibration source localization algorithm using pixel-level short-time Fourier transforms for drone localization that can only extract the drone's propeller region in various outdoor environments.

B. Super-telephoto video-shooting system

Figure 2 shows an overview of a super-telephoto mirror-drive video-shooting system for remote drone surveillance that we used in the experiment. In the telephoto video-shooting, the acquisition of plenty of light is so crucial

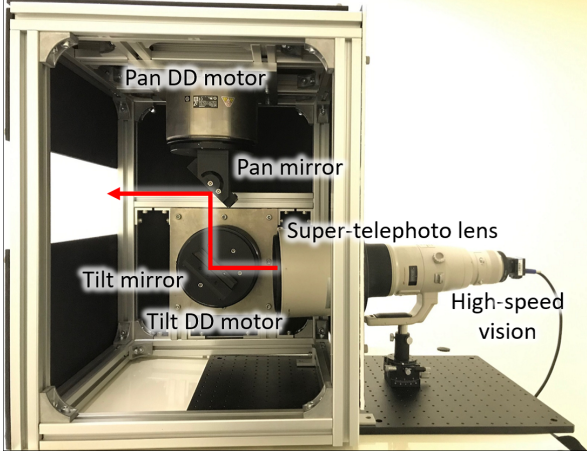


Fig. 2. Super-telephoto mirror-drive tracking system.

that monochrome image sensors that have higher sensitivity than color sensors are used. In this system, 8-bit 720×540 images can be captured at 500 fps with a 2 ms exposure, and data transfer is performed at high-speed through a USB 3.0 interface using a USB 3.1 camera (DMKBUX287, Imaging Source), whose sensor size and pixel-pitch are 4.8×3.6 mm and $6.9 \times 6.9 \mu\text{m}$. By mounting a super-telephoto lens (EF800 mm F5.6LIS USM, Canon), super-telephoto video-shooting with a focal length $f = 800$ mm can be performed. A 2-DOF mirror-drive that allows pan-tilt rotation of the viewpoint for the camera is installed on the camera head in advance. Specifically, a high-precision planar mirror with profile irregularity $\lambda/4$ that allows tilt rotation is installed in front of the camera head, and the same mirror that allows pan rotation is installed above another mirror. Both mirrors' size and weight are $100 \times 100 \times 15$ mm and 335 g, respectively. The mirrors' angles of pan and tilt are controlled by sizeable direct-drive motors (SGM7F-25C7A11, Yaskawa). Although this motor diameter is 175 mm, and weight is 15 kg, rotation control can be performed at high output torque with high accuracy, owing to the specification of repeatability 6.30×10^{-6} rad, rated angular acceleration 2250 rad/s² and encoder resolution 3.74×10^{-7} rad. These mirror angles are controlled by a Mechatrolink III interface board (SY-M3-01, Systech) communicative computer with a specialized driver. This system can capture images in the range of angles 20×20 degrees by controlling the mirror angles. In contrast, only one camera in these setting can do 0.34×0.25 degrees. By constructing them, telephoto object searching and tracking in a wide range can be executed based on high-speed visual feedback control.

C. Drone searching and tracking algorithm using pixel-level vibration extraction

Although drone localization algorithms using pixel-level digital filters [2], [3], [12] can robustly localize drones in

TABLE I
EXECUTION TIMES FOR 720×540 IMAGES CAPTURED AT 500
FPS (UNIT: MS).

K	8	16	32	64	128
(a)	16	32	64	128	256
(b)–(e)	0.964	2.007	4.429	9.619	22.908

complicated backgrounds, it is difficult for the algorithm to respond quickly when the target frequency is changed, and frequency filtering is about to start operating because pixel-level IIR filters operate based on recursive calculations as a premise for continuous data acquisition and known target frequency. In this study, the viewpoint was changed periodically, because it causes detection latency. On the other hand, short-time Fourier transform algorithms based on specific data in a period can detect a drone in low latency, compared to an IIR filter. Therefore, we implemented a pixel-level short-time Fourier transform algorithm that can simultaneously calculate multiple frequency components, regardless of the previous computation results. The region of the drone's propellers was extracted by evaluating whether there is a high peak frequency around the target frequency domain.

To extract the pixels in which the frequency f_t and its margin δf_t corresponding to the frequency band of the drone's propeller rotation in the frames captured by a high-speed vision, a short-time Fourier transform is executed for luminance value signals for all pixels as a pixel-level signal processing step. The algorithm details are as follows:

(a) HFR image accumulation:

Input images $I(x, y, k\Delta t)$ with K frames are captured at the time $t = k\Delta t$ of a high-speed vision at a high frame rate of f . $\Delta t = 1/f$ is the frame cycle time. When K frames have been accumulated, the following process (b) starts with multi-thread processing.

(b) Computation of the STFT images:

For accumulated images with K frames, the STFT images $F(x, y, k\Delta t)$ are computed as the time-frequency responses of luminance signals at each pixel at the time $t = k\Delta t$.

$$\begin{aligned} F(x, y, k\Delta t) &= (F_0(x, y, k\Delta t), \dots, F_{K-1}(x, y, k\Delta t)) \\ &= \text{STFT}(I(x, y, k\Delta t), \dots, I(x, y, (k+K-1)\Delta t)). \end{aligned} \quad (1)$$

(c) Computation of peak frequency image and its spectrum image:

In an outdoor environment, there are many objects that move at low frequency. To separate these objects from the drone's propellers, we set a lower end frequency of f_0 . By searching the maximum values of the STFT image at pixel (x, y) excluding the low frequency components under f_0 , the maximum power spectrum image $F_p(x, y, k\Delta t)$ and peak

frequency image $P(x, y, k\Delta t)$ were computed.

$$F_p(x, y, k\Delta t) = \max_{|\frac{k}{2K}f| < f_0} \mathbf{F}(x, y, k\Delta t), \quad (2)$$

$$P(x, y, k\Delta t) = \frac{f}{2K} \arg \max_{|\frac{k}{2K}f| < f_0} \mathbf{F}(x, y, k\Delta t). \quad (3)$$

(d) Computation of normalized peak frequency images:

The luminance values of the captured images were different at each viewpoint, which resulted in low accuracy when using the same threshold for the detection of target vibrations, the ratio of the peak frequency intensity image $F_r(x, y, k\Delta t)$ was computed.

$$F_r(x, y, k\Delta t) = \frac{F_p(x, y, k\Delta t)}{\sum_{i=0}^{K/2-1} F_i(x, y, k\Delta t)}. \quad (4)$$

(e) Processing of the vibration region extracted image:

When a peak frequency at pixel (x, y) was in the range of the target frequency margin δf_t , by thresholding the normalized STFT signal at the peak frequency with a threshold θ at pixel (x, y) , the vibration region $V(x, y, k\Delta t)$ for the frequency f_t and margin δf_t was extracted.

$$V(x, y, k\Delta t) = \begin{cases} 1 & (|P(x, y, k\Delta t) - f_t| < \delta f_t \\ & \wedge F_r(x, y, k\Delta t) \geq \theta) \\ 0 & (\text{otherwise}) \end{cases}. \quad (5)$$

(f) Computation of the centroids of the vibration region image:

The position of the centroids of the vibration region image $(c_x(k\Delta t), c_y(k\Delta t))$ was computed by using the 0th and 1st moment features, $M_{00}(k\Delta t)$ and $M_{10}(k\Delta t)$, $M_{01}(k\Delta t)$.

$$M_{00}(k\Delta t) = \sum_{x,y} V(x, y, k\Delta t), \quad (6)$$

$$M_{10}(k\Delta t) = \sum_{x,y} xV(x, y, k\Delta t), \quad (7)$$

$$M_{01}(k\Delta t) = \sum_{x,y} yV(x, y, k\Delta t), \quad (8)$$

$$(c_x(k\Delta t), c_y(k\Delta t)) = \left(\frac{M_{10}(k\Delta t)}{M_{00}(k\Delta t)}, \frac{M_{01}(k\Delta t)}{M_{00}(k\Delta t)} \right). \quad (9)$$

(g) The angles of the pan-tilt mirror control:

Figure 3 shows how pan-tilt mirrors are controlled. The angles of the pan and tilt mirrors are controlled based on the results of the 0th moment features $M_{00}(k\Delta t)$ (the number of detected pixels). Without detected pixels ($M_{00}(k\Delta t) = 0$), the mirror angles are changed at the next viewpoint for panorama searching. With detected pixels ($M_{00}(k\Delta t) \neq 0$), the mirror angles are controlled based on the difference between centroids of the vibration image and the center of the image using P control. Thus, the target vibration source can always be captured at the center position.

The computer (TEGSTAR CPU Intel Xeon W-2145 CPU @3.70 GHz, RAM 32.0 GB, OS Windows10 64-bit,

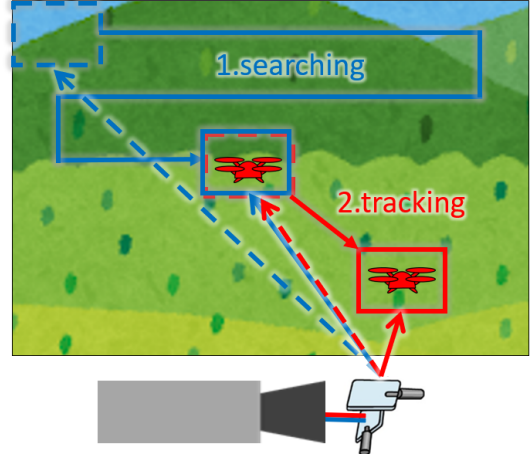


Fig. 3. The concept image of mirror control.

TEGARA) was used for real-time image processing and direct-drive motor control. Also, a GPGPU-board (GeForce RTX 2080Ti, NVIDIA) was loaded on this computer as an accelerator for pixel-level short-time Fourier transform processing, which cannot be performed by only CPU computation in real-time. Table I shows the execution times for (a) Image accumulation and (b)–(g) processing using 720×540 resolution images and K frames acquisition time for 500 fps video-shooting when the number of frames for short-time Fourier transform K is 8, 16, 32, 64, and 128. Also, the execution time scales vary linearly with image resolution. In this algorithm, while (b)–(g) are processed, (a), image acquisition is executed simultaneously by multi-thread processing. Execution times for processing (b)–(e) are much lower than that for processing (a), and this algorithm's output cycle time is almost influenced by the image acquisition in (a). That is why the output cycle time is K/f s, and the output rate is reciprocal.

IV. SUPER-TELEPHOTO DRONE SEARCHING AND TRACKING EXPERIMENT

We implemented a real-time drone searching and tracking experiment using a super-telephoto mirror-drive video-shooting system that we mentioned in Section III. The drone used in the experiment was a DJI Phantom4 with four 270 mm dual-blade propellers, whose diagonal dimension is 350 mm. When it flies, its propellers rotate in the range of 80–110 rpm. The target frequency was set to $f_t = 190$ Hz and $\delta f_t = 30$ Hz corresponding to twice the revolution speed of the propellers because the propellers are dual-blade. Figure 4 shows the experiment environment. A drone flies approximately 1 km away from the mirror-drive video-shooting system with an 800 mm focal length lens in an outdoor environment. To shorten the station time per viewpoint and accelerate the



Fig. 4. Experiment overview in telephoto drone tracking experiment.

control rate, K frames for short-time Fourier transform is set to 16. From the parameters mentioned previously, the control rate was estimated to be about 31.3 Hz ($500 (= f) / 16 (= K)$), and the range of captured images at one viewpoint is 6×4.5 square meters in 1 km distance. The threshold for the value of the peak frequency's power spectrum and low-end frequency is set to $\theta = 0.15$ and $f_0 = 50$ Hz. By changing the mirror angles in the range of ± 10 degrees, the range for drone surveillance can be expanded approximately 350×350 m 2 . In this experiment, the view angle range of captured panorama images is set to ± 1.5 degrees. Figure 5 shows the searching and tracking results of input images, detected region images and panorama images at $t = 5, 15, 25, 35, 45$ and 55 s. The drone is searched, and no vibration region is detected at $t = 5$ s because it does not fly in the view range. At $t = 15, 25, 35, 45$ and 55 s, a flying drone at a 1 km distance is always tracked around the center of images. Figure 6 shows time-series changes of the angles of the mirrors, the center coordinate value of the detected region images, and the number of detected pixels for $t = 0\text{--}55$ s. It can be understood that the duration of searching mode is $t = 0\text{--}7$ s and the tracking mode is $t = 7\text{--}55$ s and drone is consistently tracked in the center of images long distances in real-time from the graph, too. Figure 7 shows the xy -trajectories based on the centroids of the vibration region images for $t = 7\text{--}55$ s. It is estimated that the drone was flown in the range of an area spanning 28×18 square meters at a 1 km distance. Through this challenging 1-km-distance drone tracking experiment, the effectiveness of the proposed algorithm is shown.

Although stable localization is achieved in this experiment, localization accuracy depends on weather conditions, especially in longer-range telephoto video-shooting such as 3 km. In bright and sunny conditions, we should take various steps, including the construction of a robust system with heat haze. Heat haze is caused by the difference between atmospheric temperatures. There is a possibility that such

a noise component is detected as a vibration region by mistake. On the contrary, in dark and cloudy conditions, the acquisition of sufficient light is difficult, and drones may not be detected. That is why a revised algorithm that is robust with such noise is required in more challenging conditions.

V. CONCLUSION

We propose a vibration-based super-telephoto flying drone searching and tracking method using a mirror-drive telephoto video-shooting system that can extract only high-speed revolutions from flying drones and tracks the center position of propellers based on the centroids of detected images. It is confirmed that drones can be tracked at approximately a 1 km distance over a wide area, even in case of the presence of a few noisy images in the sequences.

In the future, we will try to implement a more robust system in a variety of environments such as harsh weather conditions and complicated backgrounds by combining this algorithm and other filtering methods. Also, this proposed algorithm only focuses on time-series variations, and it cannot separate the drone's propeller region and other vibration sources. It may detect flapping wings of flying birds. To prevent such failures, we will construct a dynamics and appearance identification system for robust surveillance.

ACKNOWLEDGMENT

This research was supported in part by the Strategic Information and Communications R&D Promotion Programme (SCOPE) (No.181608001), Japan Ministry of Internal Affairs and Communications, Japan.

REFERENCES

- [1] Anti-Drone Market by Technology (Laser, Kinetic, and Electronics), Application (Detection, Detection & Disruption), Vertical (Military & Defense, Homeland Security, and Commercial), and Geography - Global Forecast to 2024
- [2] M. Jiang, T. Aoyama, T. Takaki, and I. Ishii. "Pixel-level and Robust Vibration Source Sensing in High-frame-rate Video Analysis," *Sensors*, vol. 16, no. 11, pp. 1842, 2016.
- [3] M. Jiang, Q. Gu, T. Aoyama, T. Takaki, and I. Ishii. "Real-time Vibration Source Tracking Using High-speed Vision," *IEEE Sensors J.*, vol. 17, pp. 1513–1527, 2017.
- [4] I. Ishii, Y. Nakabo, and M. Ishikawa, "Target Tracking Algorithm for 1ms Visual Feedback System Using Massively Parallel Processing," in *Proc. IEEE Int. Conf. Robot. Automat.*, pp. 2309–2314, 1996.
- [5] I. Ishii, T. Tatebe, Q. Gu, Y. Morio, T. Takaki, and K. Tajima. "2000 fps Real-time Vision System with High-frame-rate Video Recording", in *Proc. IEEE Int. Conf. Robot. Automat.*, pp. 1536–1541, 2010.
- [6] T. Yamazaki, H. Katayama, S. Uehara, A. Nose, M. Kobayashi, S. Shida, M. Odahara, K. Takamiya, Y. Hisamatsu, S. Matsumoto, L. Miyashita, Y. Watanabe, T. Izawa, Y. Muramatsu, and M. Ishikawa. "A 1ms High-speed Vision Chip with 3D-stacked 140GOPS Column-parallel PEs for Spatio-temporal Image Processing," in *Proc. Int. Solid-State Circ. Conf.*, pp. 82–83, 2017.
- [7] K. Shimasaki, T. Okamura, M. Jiang, T. Takaki, and I. Ishii, "Real-Time High-speed Vision-based Vibration Spectrum Imaging," in *Proc. IEEE/SICE Int. Symp. Sys. Integr.*, pp. 474–477, 2019.
- [8] K. Shimasaki, M. Jiang, T. Takaki, I. Ishii, and K. Yamamoto, "HFR-Video-Based Honeybee Activity Sensing Using Pixel-Level Short-Time Fourier Transform," in *Proc. IEEE SENSORS 2018*, pp. 1–4, 2018.



Fig. 5. The result of telephoto drone searching and tracking experiment.

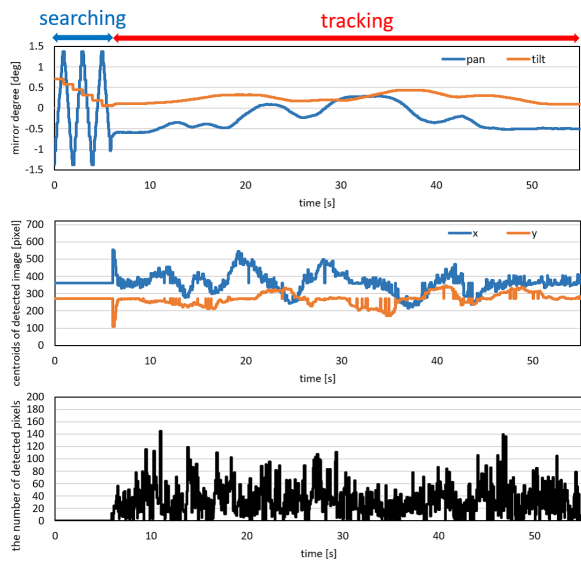


Fig. 6. The transition of mirror angles, centroids of detected images, and the number of detected pixels.

- [9] I. Ishii, T. Ichida, Q. Gu, and T. Takaki, "500-fps Face Tracking System," *J. Real-time Image Proc.*, vol. 8, no. 4, pp. 379–388, 2013.
- [10] M. Jiang, Y. Gu, T. Takaki, and I. Ishii, "High-frame-rate Target Tracking with CNN-based Object Recognition," in *Proc. IEEE/RSJ Int. Conf. Intelli. Robot. Sys.*, pp. 599–606, 2018.
- [11] K. Okumura, K. Yokoyama, H. Oku, and M. Ishikawa, "1ms Auto Pan-Tilt Video Shooting Technology for Objects in Motion Based on Saccade Mirror with Back-ground Subtraction," *Advan. Robot.*, vol. 29, no. 7, pp. 457–468, 2015.
- [12] K. Shimasaki, M. Jiang, T. Takaki and I. Ishii, "Real-Time Multicopter Detection Using Pixel-Level Digital Filters for Frame-Interpolated High-Frame-Rate Images," in *Proc. IEEE/ASME Int. Conf. Advan. Mechatr.*, pp. 304–309, 2018.

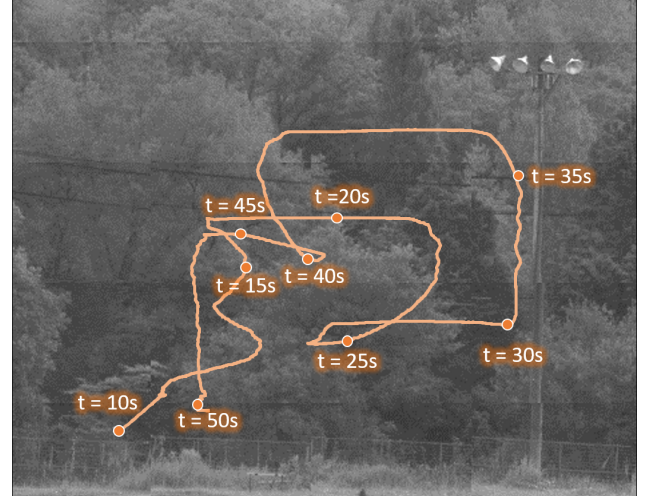


Fig. 7. A flying drone trajectory in real-time tracking.

- [13] J. Drozdowicz, M. Wielgo, P. Samczynski, K. Kulpa, J. Krzonkalla, M. mordzonek, M. Bryl, and Z. Jakielaszek, "35 GHz FMCW Drone Detection System," in *Proc. Int. Radar Symp.*, pp. 1–6, 2016.
- [14] J. Kim, C. Park, J. Ahn, Y. Ko, J. Park, and Z. J. Gallagher, "Real-time UAV Sound Detection and Analysis System," in *Proc. IEEE Sensors Appli. Symp.*, pp. 1–5, 2017.
- [15] S. Pavani, A. Delgado-Gomez, and A. Frangi, "Gaussian weak classifiers based on co-occurring Haar-like features for face detection," *Patt. Anal. Appl.*, vol. 17, no. 2, pp. 431–439, 2014.
- [16] B. Wu, C. Kao, C. Jen, Y. Li, Y. Chen, and J. Juang, "A Relative-discriminative-histogram-of-oriented-gradients-based Particle Filter Approach to Vehicle Occlusion Handling and Tracking," *IEEE Trans. Industr. Electr.*, Vol. 61, No. 8, pp. 4228–4237, 2014.
- [17] C. Aker and S. Kalkan, "Using Deep Networks for Drone Detection," in *Proc. IEEE Int. Conf. Advan. Video Signal Based Surveillance*, pp. 1–6, 2017.